**PAPER • OPEN ACCESS**

# Atomic scale structure and its impact on the band gap energy for Cu$_2$Zn(Sn,Ge)Se$_4$ kesterite alloys

View the article online for updates and enhancements.

# Journal of Physics: Energy

**PAPER**

# Atomic scale structure and its impact on the band gap energy for $Cu_2Zn(Sn,Ge)Se_4$ kesterite alloys

Konrad Ritter[1,2,8] [ID], Stefanie Eckner[1,2], Cora Preiß[2], Galina Gurieva[3] [ID], Thomas Bischoff[4,5], Edmund Welter[6], Silvana Botti[4] [ID], Susan Schorr[3,7] [ID] and Claudia S Schnohr[1,2] [ID]

1 Felix-Bloch-Institut für Festkörperphysik, Universität Leipzig, Linnéstraße 5, 04103 Leipzig, Germany
2 Institut für Festkörperphysik, Friedrich-Schiller-Universität, Max-Wien-Platz 1, 07743 Jena, Germany
3 Institut für Festkörpertheorie und -optik, Friedrich-Schiller-Universität Jena and European Theoretical Spectroscopy Facility, Max-Wien-Platz 1, 07743 Jena, Germany
4 Chaire de Simulation à l'Echelle Atomique, Ecole Polytechnique Fédérale de Lausanne, CH-1015 Lausanne, Switzerland
5 Deutsches Elektronen-Synchrotron DESY - A Research Centre of the Helmholtz Association, 22607 Hamburg, Germany
6 Helmholtz-Zentrum Berlin für Materialien und Energie, Hahn-Meitner-Platz 1, 14109 Berlin, Germany
7 Institut für Geologische Wissenschaften, Freie Universität Berlin, Malteserstr. 74-100, 12249 Berlin, Germany
8 Author to whom any correspondence should be addressed.

## Abstract

Kesterite based materials gain more and more relevance in the pursuit of affordable, efficient and flexible absorber materials for thin film photovoltaics. Alloying $Cu_2ZnSnSe_4$ with Ge could allow controlled band gap engineering as already established for $Cu(In,Ga)(S,Se)_2$ based solar cells. This study investigates the local atomic arrangements of $Cu_2Zn(Sn,Ge)Se_4$ alloys by means of low temperature Extended x-ray Absorbtion Fine Structure Spectroscopy. The element specific bond lengths are used together with x-ray diffraction data to derive the anion positions of the different local configurations. *Ab initio* theoretical calculations are performed to predict the influence of structural parameters such as anion position and lattice constants on the band gap energy. Combining the results of the experimental and theoretical studies suggests that the overall influence of the structural changes on the band gap bowing due to alloying is significant yet smaller than the total non-linear change of the band gap energy. Consequently, it is concluded, that band gap bowing stems from both structural and electronic changes.

## 1. Introduction

$Cu_2ZnSnS_4$ and $Cu_2ZnSnSe_4$, typically referred to as kesterites, are well investigated quaternary semiconductors. Their optical and electrical properties generate interest in several fields, amongst which photovoltaics may be the most prominent [1–3]. Kesterites usually consist of earth abundant and non-toxic elements, which increases their value to a market that until today relies on sometimes toxic, rare earth materials. However, the current record of 12.6% conversion efficiency [4] is still well below the theoretical limit of around 30% [5]. This gap in performance mostly stems from a severe open circuit voltage deficit and may have several different reasons, including the bulk structure of the kesterite absorber itself [6]. Various studies have shown that the best kesterite devices are usually Cu poor and Zn rich [1]. However, secondary phases and compositional fluctuations are typical features of non-stoichiometric kesterites and could likely be detrimental to the conversion efficiency [7]. The Cu-Zn disorder, another characteristic feature of kesterite materials [8], has also been discussed as the source of the open circuit voltage deficit [9]. Furthermore, different types of point defects have been observed experimentally [10] and Sn in particular is a potentially multivalent element, that has been predicted to create deep defects, thus reducing the conversion efficiency by increasing the recombination rate of charge carriers [11–13].

Research on $Cu(In,Ga)(S,Se)_2$ based solar cells has shown that replacing or mixing of elements on certain lattice positions may improve the device performance drastically by enabling precise band gap engineering.

Partially or completely replacing any element in the kesterite structure may also have beneficial effects on device performance and several different methods are investigated to drive development of marketable kesterite solar cells [14]. While the current record device has a $Cu_2ZnSn(S,Se)_4$ absorber, there are many promising approaches to replace different amounts of Sn with Ge, ranging all the way from fine doping up to complete substitution [15–19]. One of these approaches with a Ge content (Ge/Ge+Sn) of 0.22 even enabled a conversion efficiency of 12.3% [19] being very close to the current record of 12.6% [4].

Germanium is a non-toxic and arguably earth abundant element [20], but its atomic and ionic radii are about 15% and 25% less than those of Sn [21]. Therefore, a significant change in both the local atomic structure and the long range crystallographic structure can be expected. Pure $Cu_2ZnGeSe_4$ also crystalizes in the kesterite structure (space group $I\bar{4}$) but with about 3% smaller lattice constants than $Cu_2ZnSnSe_4$ [22]. In $Cu(In,Ga)Se_2$ and $Cu(In,Ga)S_2$, the different radii of the substituting elements further have a strong effect on the local atomic arrangements around the Se or S anions [23, 24]. This atomic scale structure, specifically the anion displacement, is a key factor for the band gap energy not only for $Cu(In,Ga)Se_2$ and $Cu(In,Ga)S_2$ [25, 26] but also for kesterite materials [27]. Hence, a detailed knowledge about the local atomic arrangements around the Se anions is mandatory to understand the changes imposed by replacing Sn with Ge.
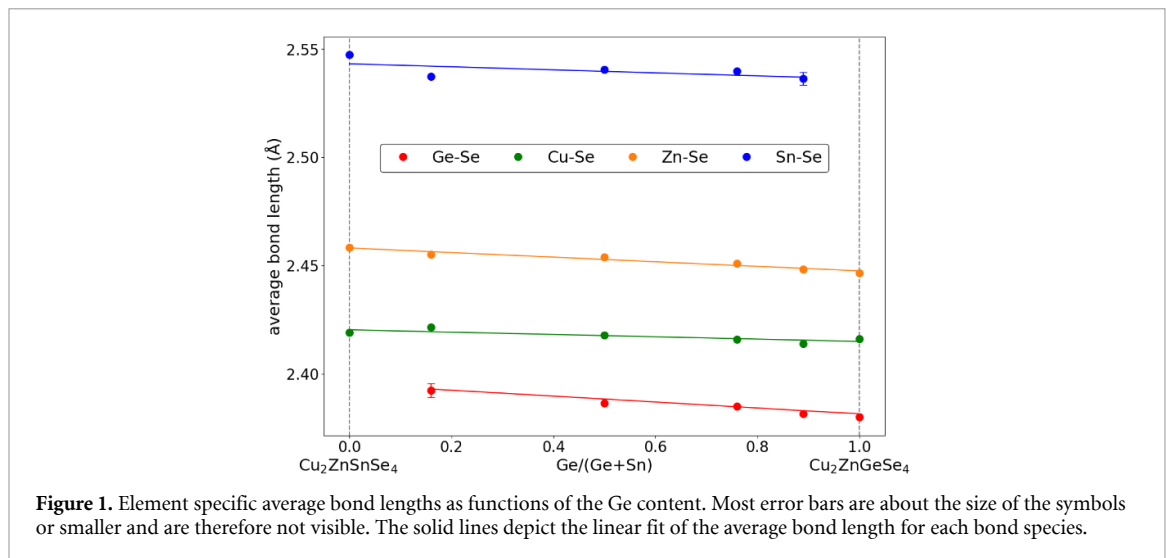
This work combines Extended x-ray Absorbtion Fine Structure Spectroscopy (EXAFS) and *ab initio* theoretical calculations to determine the atomic scale structure of $Cu_2Zn(Sn,Ge)Se_4$ alloys as a function of the Ge content and to estimate the impact of the different structural changes on the band gap energy. EXAFS provides element specific average bond lengths and bond length variations and has already been successfully used to study numerous ternary semiconductor alloys [28], $Cu(In,Ga)Se_2$, $Cu(In,Ga)S_2$ and related materials [23, 24, 28, 29] and $Cu_2(Zn,Fe)SnS_4$ [30]. The dependence of the band gap energy on the anion position has previously been calculated by density functional theory based methods for $CuInS_2$ and $CuInSe_2$ [25] and for $Cu_2ZnSnS_4$ [27].

## 2. Experimental

Six different $Cu_2Zn(Sn,Ge)Se_4$ powder samples with Ge/(Ge+Sn) (GGS) between 0 and 1 were synthesized by solid state reaction of pure elements as described for pure $Cu_2ZnGeSe_4$ in [22]. The first step of synthesis places the samples at 700 °C for 240 h , followed by a homogenization and another 240 h annealing step at 700 °C. Both synthesis and annealing are performed in vacuum. During the in weigh 2% Selenium shot is added to the ampoule, to account for the possible evaporation during the sealing of the tube. No additional powders of Se or SnSe are added at any further step. The resulting material was characterized with x-ray diffraction (XRD), wavelength dispersive x-ray spectroscopy, back scatter electron micrographs, Raman spectroscopy and for the pure $Cu_2ZnGeSe_4$ with neutron powder diffraction [22]. All samples are single phase and exhibit the kesterite structure. Prior to the EXAFS measurements, the powder samples were diluted with graphite , milled in a ball mill and pressed into pellets with 5 mm diameter, to ensure mechanical stability and to enable handling during the experiments. For each sample, two sets of pellets were prepared with the amount of sample material optimized for measurement of either the Cu, Zn, and Ge K-edges or the Sn K-edge.

Low temperature EXAFS measurements took place at the P65 beamline of PETRA III at DESY in Hamburg, Germany [31]. Spectra were taken at the Cu, Zn, Ge and Sn K-edge (8979 eV, 9659 eV, 11103 eV and 29200 eV, respectively) in transmission mode. A liquid helium flow-through cryostat ensured the stability of the measurement temperature of 18 K to better than 1 K. Low temperature was chosen, to ensure the best possible signal to noise ratio and the highest precision for the determination of the structural parameters. The energy scales of different measurements were aligned using the reference spectra measured simultaneously with the main samples. The reproducibility of measured data was confirmed for at least one sample at each edge by remeasuring with identical set up.

Primary data processing including background subtraction and normalization was carried out with the Demeter software package [32]. The data quality allowed a Fourier transformation window in k-space starting at 3 Å$^{-1}$ and extending up to 15 Å$^{-1}$ for Zn and Ge and 14 Å$^{-1}$ for Sn. At the Cu edge the upper limit is given by the Zn edge starting beyond 12 Å$^{-1}$. The tapering parameter of the window function was 2 Å$^{-1}$ in all cases. Phase shifts and scattering amplitudes were calculated using Feff9 [33]. Final fitting in R-space of the mean value $d$ (average bond length) and the width $\sigma^2$ (bond length variation) of the nearest neighbour distance distribution was achieved through the scripting library Larch [34]. The higher ($\geq 3$) cumulants were tested and identified to be negligible and were thus set to zero. For final results, the fits were carried out with multiple k-weights of $k^2$, $k^3$ and $k^4$. The R-window was [1.4 Å, 2.8 Å] at the Cu-edge, [1.6 Å, 2.7 Å] at the Zn-edge, [1.4 Å, 2.7 Å] at the Ge-edge and [1.6 Å, 2.8 Å] at the Sn-edge with a tapering parameter of 0.5 Å for Zn and Ge and 0.6 Å for Cu and Sn. For the amplitude reduction factor $S_0^2$ and the

**Figure 1.** Element specific average bond lengths as functions of the Ge content. Most error bars are about the size of the symbols or smaller and are therefore not visible. The solid lines depict the linear fit of the average bond length for each bond species.

energy threshold $E_0$ the average value over all samples at one edge was determined and both values were fixed accordingly. Furthermore, all the above parameters were systematically varied to test their individual influence on the fitting parameters. Additionally, the influence of the Fourier transformation parameters on the results was investigated. The dependencies of the fitted average bond length on these analysis settings was then used to estimate the overall uncertainties of the final results.

## 3. Theoretical calculations

Values of band gaps in excellent agreement with experiments can be obtained using the Heyd-Scuseria-Ernzerhof (HSE06) [35, 36] hybrid functional, as implemented in the Vienna *ab initio* simulation package (Vasp) [37, 38]. The selected exchange-correlation functional yields band structures of kesterites in excellent agreement with experiment [27]. We performed here calculations of the fundamental band gap at $\Gamma$ for $Cu_2ZnSnSe_4$ and $Cu_2ZnGeSe_4$ (as well as $Cu_2ZnSnS_4$ and $Cu_2ZnGeS_4$), starting from the experimental geometry, and then varying one by one the $x$, $y$, $z$ coordinates of the anion position, the volume $V$, and the tetragonal distortion $\eta = \frac{c}{2a}$. We used the PAW [39, 40] datasets of version 5.2 with a cutoff of 520 eV and $\Gamma$-centered $k$-point grids, as dense as required to ensure an accuracy of 2 meV/atom in the total energy.
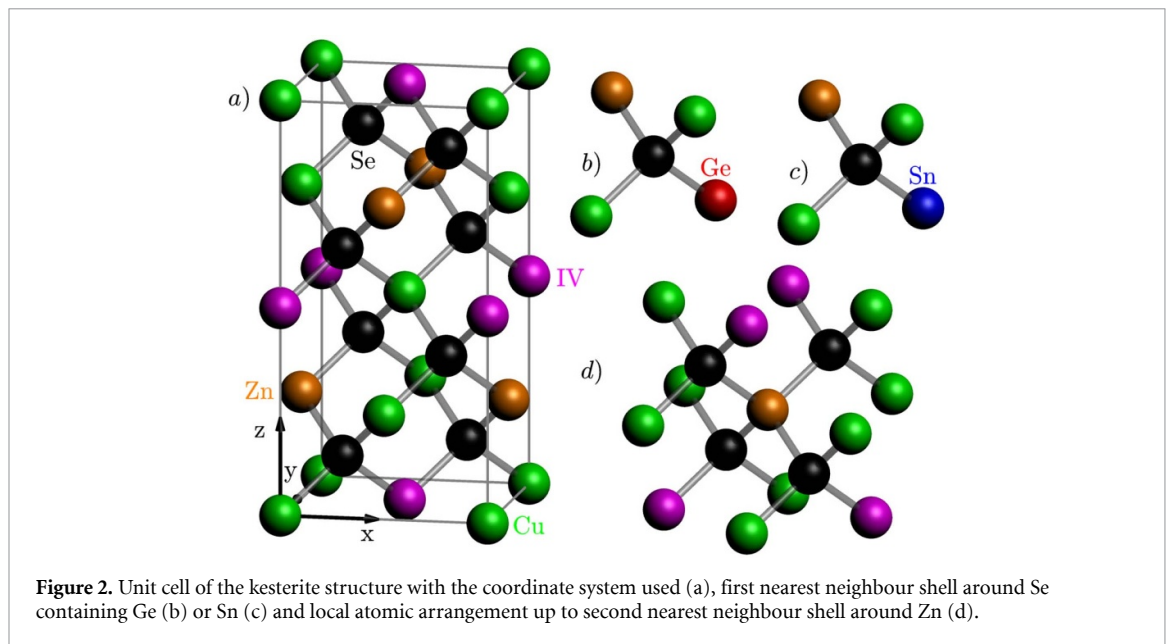
The variation of the band gap with changing structural parameters can be written as

$$\Delta E_g = \frac{\partial E_g}{\partial x}\Delta x + \frac{\partial E_g}{\partial y}\Delta y + \frac{\partial E_g}{\partial z}\Delta z$$
$$+ \frac{\partial E_g}{\partial V}\Delta V + \frac{\partial E_g}{\partial \eta}\Delta \eta, \tag{1}$$

assuming that the linear approximation is valid for small structural deformations. The range of validity of the linear approximation and the values of the partial derivatives can be directly extracted from the calculations of $E_g$.

## 4. Element specific bond lengths

The element specific average bond lengths obtained from the EXAFS measurements are depicted in figure 1. The data and fits for all samples are shown in the supplementary material (stacks.iop.org/JPENERGY/ 02/035004/mmedia). The estimated overall uncertainties, containing the influence of all analysis parameters and the reported uncertainty of the fit, are smaller than 0.002 Å for all four cations and therefore not visible in figure 1. The only exceptions are the Ge-Se bond length for the sample with the least amount of Ge and the Sn-Se bond length for the least amount of Sn, their error bars are about 0.003 Å due to the low signal from the respective element. For each bond species, the average bond length decreases with increasing Ge content. This trend is well represented by a linear function in all cases. However, the individual average bond lengths only change less than 0.5%, while the global lattice constants are reduced by about 3% when going from the pure $Cu_2ZnSnSe_4$ to the pure $Cu_2ZnGeSe_4$ [22, 41, 42]. This behaviour is well known for numerous ternary

**Figure 2.** Unit cell of the kesterite structure with the coordinate system used (a), first nearest neighbour shell around Se containing Ge (b) or Sn (c) and local atomic arrangement up to second nearest neighbour shell around Zn (d).

and quaternary alloys of tetrahedrally coordinated compounds and indicates the preference of bond angle changes over bond length changes to accommodate the lattice mismatch between the parent materials [28].
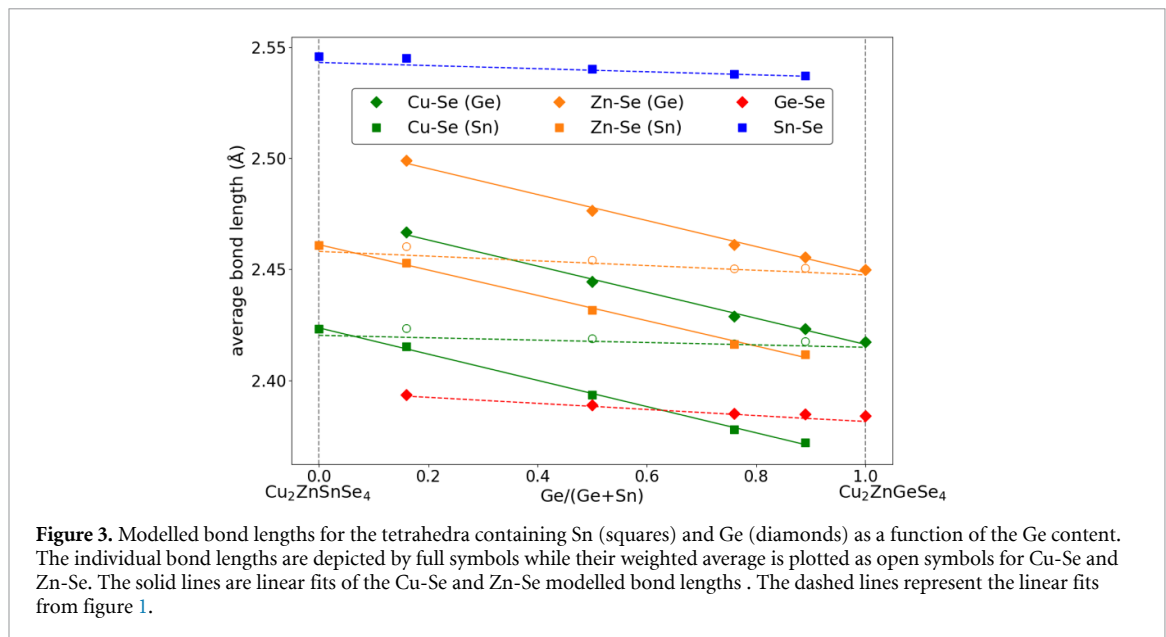
XRD measurements of the end materials $Cu_2ZnSnSe_4$ and $Cu_2ZnGeSe_4$ yield lattice positions [10, 22], whose distances are in agreement with the EXAFS results. The latter further show that the average Ge-Se bond lengths are about 0.15 Å smaller than the average Sn-Se bond lengths in the $Cu_2Zn(Sn,Ge)Se_4$ alloys, despite the fact that Sn and Ge share the same lattice site. This difference in the element specific average bond lengths induces significant variations of the local atomic arrangements, depending on whether a Ge or a Sn cation is present. In the kesterite structure, depicted in figure 2, each cation is surrounded by a first nearest neighbour shell of four Se anions. For Ge and Sn, the second nearest neighbour shell only contains Cu and Zn but no group IV element, as can be seen in figure 2(a) by considering the group IV atoms at the bottom and top of the unit cell. Therefore, Sn and Ge feature a single, well determined local atomic environment. In contrast, the second nearest neighbour shell of Cu and Zn contains four group IV elements. For Cu, this local environment can be seen around the central Cu atom of the unit cell in figure 2(a) and for Zn it is shown in figure 2(d). In the mixed materials, these four group IV elements can be any combination of Ge and Sn. This leads to five different principal configurations, where the number of Ge atoms ranges from zero to four. It has to be expected that the individual Cu-Se and Zn-Se bond lengths are different in each configuration and hence that there is a substantial difference in the local atomic scale structure depending on the type of group IV elements. However, these different configurations can not be distinguished experimentally by EXAFS. Therefore, the Cu-Se and Zn-Se bond lengths determined from the EXAFS measurements are average values of the different local configurations.

## 5. Anion positions

To model the atomic scale structure of the different local configurations, in particular the anion position, a small subunit of the kesterite structure has been considered. This subunit is a tetrahedron with Se in the center and two Cu, one Zn and one group IV atom as first nearest neighbours. It is shown in figure 2(b) and (c) for Ge and Sn as group IV element. The entire kesterite structure is made up of these two types of tetrahedra. Without loss of generality, we chose the tetrahedron in the lower left of the unit cell, resulting in the cation lattice positions Cu (0,0,0) and $(\frac{1}{2},0,\frac{1}{4})$, Zn $(0,\frac{1}{2},\frac{1}{4})$ and Sn or Ge on $(\frac{1}{2},\frac{1}{2},0)$.

The assumptions of the model are similar to those used by Balzarotti *et al* for the description of ternary III-V and II-VI zincblende alloys [43]. It is assumed, that all cations are fixed to their lattice positions. It is consequently assumed in this model, that the anion position and the lattice constants are the only structural parameters changing with the Ge content. The lattice parameters a and c have been determined by XRD as a function of Ge content. Consequently, the position of the Se within the tetrahedron is the only variable of the model.

For each composition the model consists of two tetrahedra, one with Ge and one with Sn (see figure 2(b) and (c)). The two Cu-Se bonds occurring within one tetrahedron were assumed to be equal in length, thus imposing a symmetry constraint on the Se position. The distance between a cation position and the Se

**Figure 3.** Modelled bond lengths for the tetrahedra containing Sn (squares) and Ge (diamonds) as a function of the Ge content. The individual bond lengths are depicted by full symbols while their weighted average is plotted as open symbols for Cu-Se and Zn-Se. The solid lines are linear fits of the Cu-Se and Zn-Se modelled bond lengths . The dashed lines represent the linear fits from figure 1.

position is called the modelled bond length for this bond species and the tetrahedron considered. To model the anion position in each of the two tetrahedra, the Se positions were varied until the deviation between the measured average bond lengths and the corresponding modelled bond lengths was minimized. As mentioned before, the measured Cu-Se and Zn-Se bond lengths represent a weighted average of both possible tetrahedra. Therefore, the GGS weighted average of the modelled bond lengths of the two tetrahedra was compared to the experimental value for Cu-Se and Zn-Se. The optimal modelled bond lengths are plotted and compared to the experimental bond lengths in figure 3. The modelled Sn-Se and Ge-Se bond lengths are in good agreement with the linear fit of the measured values. As expected the Cu-Se and Zn-Se bond lengths split up for the two tetrahedra and these modelled bond lengths do not match the respective measured ones. However, their GGS weighted average does fit the measured data. The modelled bond lengths therefore show excellent agreement with the measured data. All modelled bond lengths decrease with increasing GGS in accordance with the decrease in the global lattice parameters. Cu-Se and Zn-Se react far stronger to the change in GGS, which shows that these are softer bonds due to their higher ionicity compared to the IV-Se bonds. Similar findings are reported for Cu-Se and In-Se or Ga-Se in Cu(In,Ga)Se$_2$ [23]. This highlights the importance of considering the very local atomic arrangement since the GGS weighted average Cu-Se and Zn-Se bond lengths decrease less than the Ge-Se and Sn-Se bond lengths and would thus, erroneously, suggest stiffer Cu-Se and Zn-Se bonds.

Due to the difference of the individual Cu-Se and Zn-Se bond lengths, the Se positions, which are shown in figure 4, differ significantly for the Ge and Sn tetrahedron. In all cases the $x$ and $y$ coordinates are $< 0.25$ for the Sn and $\geq 0.25$ for the Ge tetrahedron. This is a direct result of the Ge-Se bond being smaller than nearly all the other bond lengths, while Sn-Se is the largest bond length in the system. The dashed lines in figure 4 are the projections of the body diagonal of the quasi-cube spanned by the cations of the tetrahedra, shown in magenta. In figure 4(a) $y$ is smaller than $x$, since the Cu-Se bond lengths are smaller than the Zn-Se bond length. In figure 4(b) the data points fall on the dashed line and hence $z = -\frac{1}{2} \cdot x + \frac{1}{4}$, which is a direct consequence of the symmetry imposed by the two equal Cu-Se bonds in each tetrahedron. Apart from these overall observations, the Se position further shifts with changing Ge content for both tetrahedra. This shift is parallel to the dashed line demonstrating that the Se positions evolve parallel to the body diagonal of the quasi-cube. Therefore, the relative distance to the group IV atom is changed and the relative distances to all other cations are adjusted accordingly. At first glance, it might be counterintuitive that all bond lengths in figure 3 decrease with increasing GGS whereas the Se position in figure 4 shifts away from the group IV atom. This is because the positions in figure 4 are relative to the tetrahedron. Looking at the Sn tetrahedron for GGS $= 0$, all bonds have their natural length of the Cu$_2$ZnSnSe$_4$ kesterite structure. When GGS rises, the tetrahedron gets smaller as the lattice parameters shrink. The Sn-Se bond is stiffer than the Cu-Se or Zn-Se bonds and therefore decreases less with GGS than the others. As a result, the relative Se position is closer to Cu and Zn and further away from Sn, even though all three types of bonds decrease. For the Ge tetrahedron it is the other way around. Its ideal state is GGS $= 1$ where all bond lengths are at their desired low. With decreasing GGS, the tetrahedron increases in size, and therefore all bonds have to stretch. As Ge-Se is stiffer than Cu-Se and Zn-Se, it does not stretch as much and therefore, the relative position of Se becomes closer to
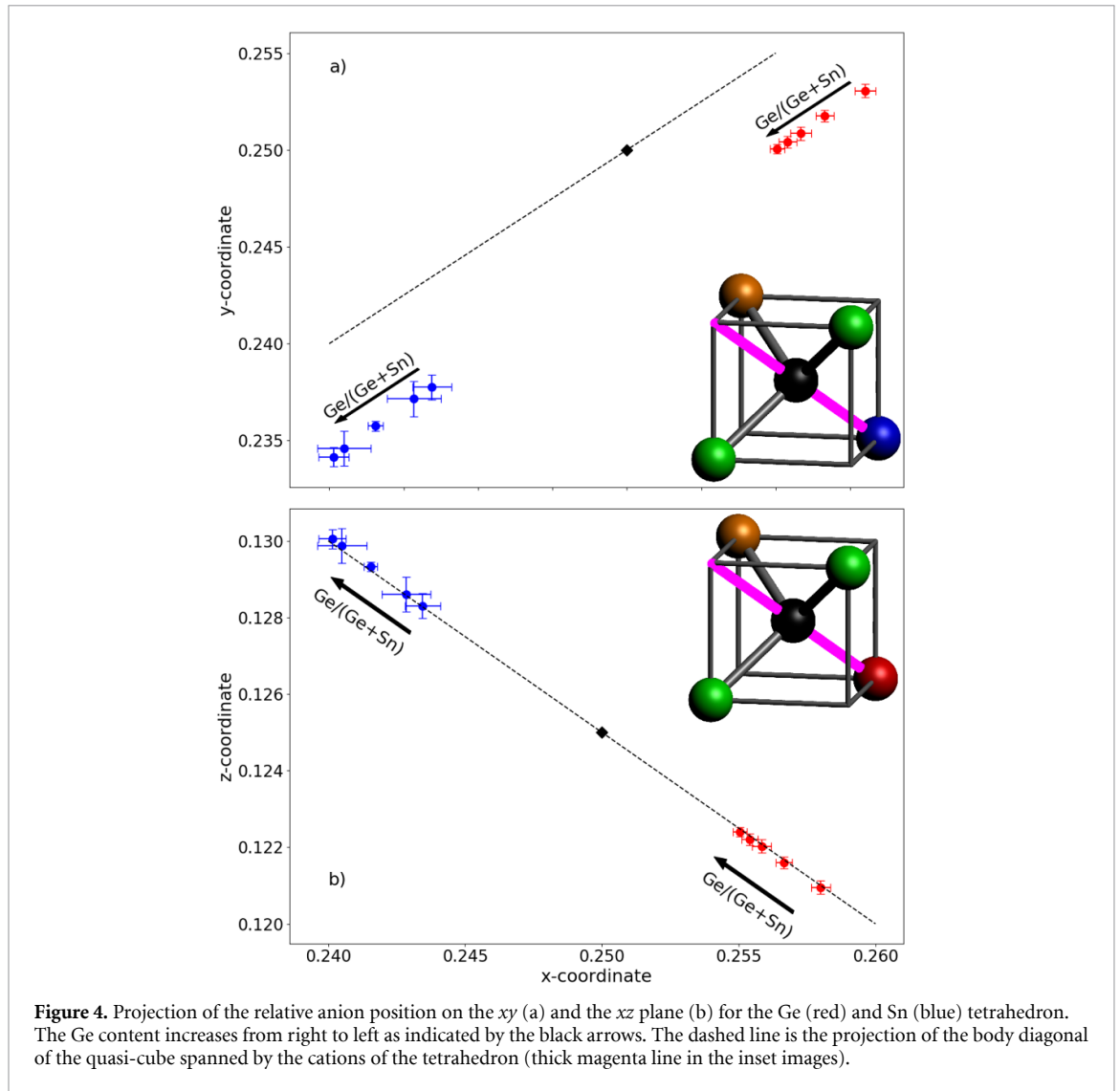
**Figure 4.** Projection of the relative anion position on the *xy* (a) and the *xz* plane (b) for the Ge (red) and Sn (blue) tetrahedron. The Ge content increases from right to left as indicated by the black arrows. The dashed line is the projection of the body diagonal of the quasi-cube spanned by the cations of the tetrahedron (thick magenta line in the inset images).

**Table 1.** Change in relative anion position $x$, $y$ and $z$ from the modelled data, change in unit cell volume $V$ and change in tetragonal distortion $\eta = \frac{c}{2a}$ from XRD measurements, all when increasing GGS from 0 ($Cu_2ZnSnSe_4$) to 1 ($Cu_2ZnGeSe_4$). Furthermore, the calculated dependence of band gap energy $E_g$ on these different structural parameters is listed corresponding to increasing GGS.

| IV | $\Delta x$ | $\Delta y$ | $\Delta z$ | $\Delta V$ (Å³) | $\Delta \eta$ | $\frac{\partial E_g}{\partial x}$ (eV) | $\frac{\partial E_g}{\partial y}$ (eV) | $\frac{\partial E_g}{\partial z}$ (eV) | $\frac{\partial E_g}{\partial V}$ (eVÅ⁻³) | $\frac{\partial E_g}{\partial \eta}$ (eV) |
|---|---|---|---|---|---|---|---|---|---|---|
| Ge | $-0.0035$ | $-0.0036$ | $0.0017$ | $-20.03$ | $-0.013$ | $20.66$ | $15.95$ | $-23.78$ | $-0.01$ | $-3.51$ |
| Sn | $-0.0038$ | $-0.0041$ | $0.0020$ | $-20.03$ | $-0.013$ | $17.80$ | $12.29$ | $-14.41$ | $-0.01$ | $-1.80$ |

Ge than to Cu and Zn. Following increasing GGS, this creates the same qualitative behaviour for Ge and Sn, only differing in starting positions.

## 6. Band gap energy

The calculated dependence of the band gap energy on the anion position $(x, y, z)$, on the unit cell volume $V$ and on the tetragonal distortion $\eta$ is presented in figure 5. Both starting values are marked as circles and represent pure $Cu_2ZnSnSe_4$ or $Cu_2ZnGeSe_4$ in good agreement with experimental values from literature [1, 44]. The calculated band gap energy changes linearly with all structural parameters. Only the tetragonal distortion creates a non linear trend in band gap energy for values of $\eta \geq 1$, especially for $Cu_2ZnSnSe_4$ (see figure 5(e)). As all samples in this study exhibit values of $\eta$ lower than 1, the linear fit in figure 5(e) was restricted to $\eta \leq 1$. The slopes determined for estimating the change in band gap energy $\Delta E_g$ are summarized in table 1. For increasing $x$ and $y$ and decreasing $z$ values, so for positions closer to the group IV element, the band gap energy increases. The reduced distance between Se and the group IV atom increases the repulsion between Sn or Ge s and Se p orbitals, thus shifting the conduction band minimum to higher energies [45]. At
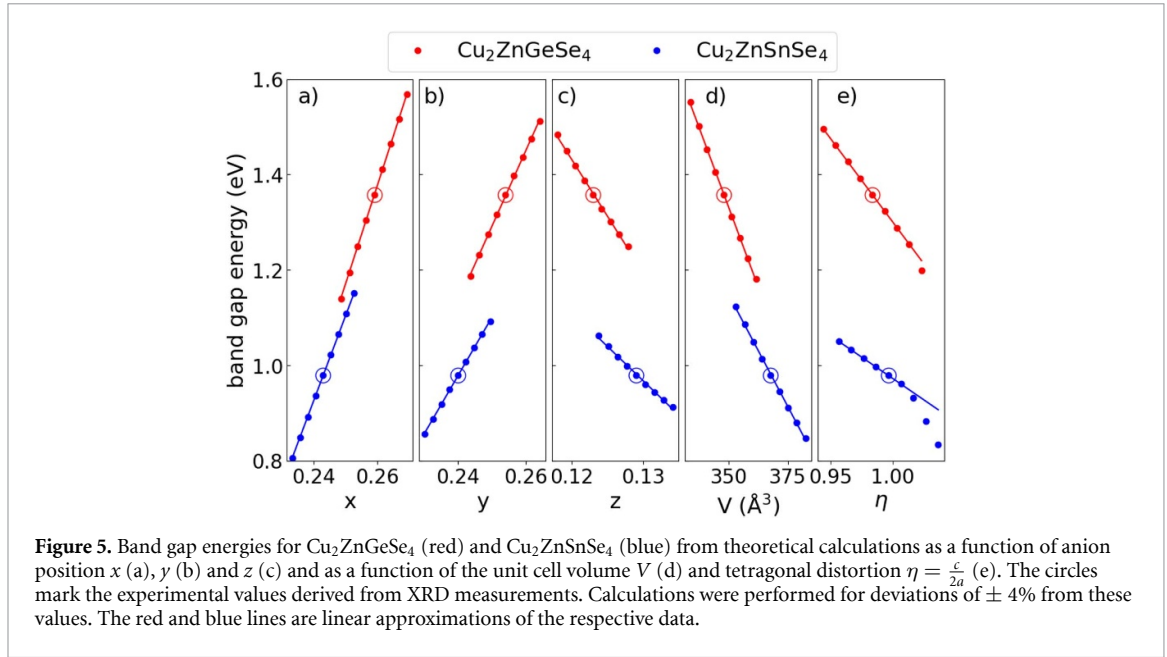
**Figure 5.** Band gap energies for $Cu_2ZnGeSe_4$ (red) and $Cu_2ZnSnSe_4$ (blue) from theoretical calculations as a function of anion position $x$ (a), $y$ (b) and $z$ (c) and as a function of the unit cell volume $V$ (d) and tetragonal distortion $\eta = \frac{c}{2a}$ (e). The circles mark the experimental values derived from XRD measurements. Calculations were performed for deviations of $\pm 4\%$ from these values. The red and blue lines are linear approximations of the respective data.

**Table 2.** Contribution of each structural parameter to $\Delta E_g$ in $eV$, when increasing GGS from 0 ($Cu_2ZnSnSe_4$) to 1 ($Cu_2ZnGeSe_4$).

| IV | $\Delta E_g^x$ | $\Delta E_g^y$ | $\Delta E_g^z$ | $\Delta E_g^V$ | $\Delta E_g^\eta$ | $\Delta E_g$ |
|---|---|---|---|---|---|---|
| Ge | $-0.072$ | $-0.057$ | $-0.041$ | $0.27$ | $0.045$ | $0.14$ |
| Sn | $-0.067$ | $-0.051$ | $-0.029$ | $0.19$ | $0.023$ | $0.06$ |

the same time, it can be expected that the valence band maximum is shifted upwards by repulsive interaction between the Cu d and Se p states, a behavior well known for $Cu(In,Ga)Se_2$ [46]. Increasing the Cu-Se distance reduces the p-d repulsion and thus lowers the valence band maximum. Both effects result in the increase of the band gap energy as the anion position is shifted towards the group IV atom. An increase in unit cell volume decreases the band gap energy. This behaviour is well known, for example from the dependency of the band gap energy on pressure or temperature [47]. Increasing tetragonal distortion also reduces the band gap energy. In all cases, the change is larger for the Ge environment than for the Sn environment since the interaction between the different orbitals is stronger for Ge than for Sn [45].

Values for $\Delta x$, $\Delta y$ and $\Delta z$ in equation (1) are derived from figure 4 by extrapolating the anion positions to GGS = 0 for the Ge tetrahedron and GGS = 1 for the Sn tetrahedron and calculating the respective differences. $\Delta V$ and $\Delta \eta$ in equation (1) are derived from the lattice parameters obtained by XRD measurements for each value of GGS. In table 1 the values of all these parameters are displayed. All five parameters are linear functions of GGS.

With this data and equation (1), the contribution for each structural parameter and the overall change in the band gap energy were calculated and are listed in table 2. Both $\eta$ and $V$ decrease with increasing GGS, which in turn increases the band gap energy. The influence of $V$ is significantly stronger and dominates the change of the entire band gap energy. In contrast, the change in anion position does decrease the band gap energy. The combined influence of all three anion coordinates, is significant but still insufficient to compensate the influence of $V$.

The band gap energy of $Cu_2Zn(Sn,Ge)Se_4$ alloys can be described by a quadratic dependence [45, 48, 49]

$$E_g = GGS \cdot E_{g,0}^{Ge} + (1 - GGS) \cdot E_{g,0}^{Sn}$$
$$- b \cdot GGS(1 - GGS) \tag{2}$$

were $E_{g,0}^{Ge}$ and $E_{g,0}^{Sn}$ denote the band gap energy of pure $Cu_2ZnGeSe_4$ and $Cu_2ZnSnSe_4$ and $b$ is the so called bowing parameter. Alternatively, the band gap energy of the alloy can be conceived as the weighted average of the band gap energies of Ge and Sn containing material with structural properties corresponding to the alloy composition

$$E_g = GGS \cdot E_g^{Ge} + (1 - GGS) \cdot E_g^{Sn}. \tag{3}$$

Following equation (1), these composition dependent band gap energies can be expressed as

$$E_g^{\mathrm{IV}}(GGS) = E_{g,0}^{\mathrm{IV}} + \Delta E_g^{\mathrm{IV}}(GGS). \qquad (4)$$

Since all structural parameters change linearly with alloy composition and since the band gap energies depend linearly on the structural parameters, equation (4) can be written as

$$E_g^{\mathrm{Ge}}(GGS) = E_{g,0}^{\mathrm{Ge}} - (1 - GGS) \cdot \Delta E_g^{\mathrm{Ge}} \qquad (5)$$

$$E_g^{\mathrm{Sn}}(GGS) = E_{g,0}^{\mathrm{Sn}} + GGS \cdot \Delta E_g^{\mathrm{Sn}} \qquad (6)$$

where $\Delta E_g^{\mathrm{Ge}}$ and $\Delta E_g^{\mathrm{Sn}}$ denote the overall change of the band gap energy of Ge and Sn containing material, respectively, when increasing GGS from 0 ($Cu_2ZnSnSe_4$) to 1 ($Cu_2ZnGeSe_4$) as given in table 2. Inserting equation (5) and (6) into equation (3) yields

$$E_g = GGS \cdot E_{g,0}^{\mathrm{Ge}} + (1 - GGS) \cdot E_{g,0}^{\mathrm{Sn}} \qquad (7)$$
$$- (\Delta E_g^{\mathrm{Ge}} - \Delta E_g^{\mathrm{Sn}}) \cdot GGS(1 - GGS).$$

Comparison with equation (2) yields the bowing parameter $b = \Delta E_g^{\mathrm{Ge}} - \Delta E_g^{\mathrm{Sn}} = 0.08\ eV$. This is smaller than most of the bowing parameters determined both experimentally and theoretically ranging from 0 up to 0.29 eV [15, 45, 48–51]. The difference between the values obtained in this study and the values reported in the literature most likely stems from the fact, that here only changes of the band gap energy were considered that result from changes of the structural parameters. However, the band gap bowing originates from both structural changes and electronic changes as discussed in detail for ternary semiconductor alloys with zincblende structure [47, 52]. The electronic changes result from charge redistribution between the anion and the different cations upon alloying and in combination with the changing structural parameters. Additionally Cu-Zn disorder has been shown to affect the band gap energy [9, 53, 54]. If the degree of Cu-Zn disorder depends on the Ge content, this could further contribute to the non linear change of the band gap and would thus represent another structural contribution to the band gap bowing, which cannot be accessed by our methodology. The bowing parameter estimated in this work clearly demonstrates that structural changes due to alloying give rise to a significant fraction of the overall band gap bowing while additional effects such as electronic changes and varying Cu-Zn disorder must account for the rest.

## 7. Conclusion

The local atomic scale structure of $Cu_2Zn(Sn,Ge)Se_4$ kesterite alloys has been studied as a function of the Ge content, by means of low temperature EXAFS measurements. All average bond lengths in this study decrease with increasing Ge content. Yet Sn-Se and Ge-Se have far lower slopes than Zn-Se and Cu-Se, as shown in a model of the local atomic structure. Anion positions resulting from said model, are vastly different depending on the type of group IV element present in the local structure around Se. They are shifted in the direction of the IV-Se bond, again showing Sn-Se and Ge-Sn to be the stiffer bonds. *Ab initio* HSE calculations show, that the band gap energy changes linearly with all structural parameters. The resulting slopes together with the anion positions allow for an estimation of the structural part of the band gap bowing parameter due to alloying as 0.08 eV.

## ORCID iDs

Konrad Ritter ⓘ https://orcid.org/0000-0003-4501-7036
Galina Gurieva ⓘ https://orcid.org/0000-0001-8609-1043
Silvana Botti ⓘ https://orcid.org/0000-0002-4920-2370
Susan Schorr ⓘ https://orcid.org/0000-0002-6687-614X
Claudia S Schnohr ⓘ https://orcid.org/0000-0002-3688-7104

# References

[1] Giraldo S, Jehl Z, Placidi M, Izquierdo-Roca V, Pérez-Rodríguez A and Saucedo E 2019 *Adv. Mater.* **31** 1806692
[2] Wallace S K, Mitzi D B and Walsh A 2017 *ACS Energy Lett.* **2** 776
[3] Sevik C and Çağin T 2010 *Phys. Rev.* B **82** 045202
[4] Wang W, Winkler M T, Gunawan O, Gokmen T, Todorov T K, Zhu Y and Mitzi D B 2013 *Adv. Energy Mater.* **4** 1301465
[5] Shockley W and Queisser H J 1961 *J. Appl. Phys.* **32** 510
[6] Liu X, Feng Y, Cui H, Liu F, Hao X, Conibeer G, Mitzi D B and Green M 2016 *Prog. Photovoltaics Res. Appl.* **24** 879
[7] Schorr S *et al* 2019 *J. Phys. Energy* **2** 012002
[8] Schorr S 2011 *Sol. Energy Mater. Sol. Cells* **95** 1482
[9] Bourdais S *et al et al* 2016 *Adv. Energy Mater.* **6** 1502276
[10] Gurieva G, Rios L E V, Franz A, Whitfield P and Schorr S 2018 *J. Appl. Phys.* **123** 161519
[11] Biswas K, Lany S and Zunger A 2010 *Appl. Phys. Lett.* **96** 201902
[12] Chen S, Walsh A, Gong X-G and Wei S-H 2013 *Adv. Mater.* **25** 1522
[13] Yee Y S, Magyari-Köpe B, Nishi Y, Bent S F and Clemens B M 2015 *Phys. Rev.* B **92** 195201
[14] Giraldo S, Neuschitzer M, Izquierdo-Roca V, Perez-Rodriguez A and Saucedo E 2018 *2018 IEEE 7th Conf. on Photovoltaic Energy Conversion* pp 3869–72
[15] Shu Q, Yang J-H, Chen S, Huang B, Xiang H, Gong X-G and Wei S-H 2013 *Phys. Rev.* B **87** 115208
[16] Giraldo S *et al* 2015 *Adv. Energy Mater.* **5** 1501070
[17] Giraldo S, Neuschitzer M, Placidi M, Pistor P, Perez-Rodriguez A and Saucedo E 2016 *IEEE J. Photovoltaics* **6** 754
[18] Collord A D and Hillhouse H W 2016 *Chem. Mater.* **28** 2067
[19] Kim S, Kim K M, Tampo H, Shibata H and Niki S 2016 *Appl. Phys Express* **9** 102301
[20] Bleiwas D I 2010 *U.S. Geological Survey Circular* **1365** (https://pubs.usgs.gov/circ/1365/)
[21] Shannon R D 1976 *Acta Crystallograph. Section* A **32** 751
[22] Gurieva G, Többens D, Valakh M Y and Schorr S 2016 *J. Phys. Chem. Solids* **99** 100
[23] Schnohr C S, Kämmer H, Stephan C, Schorr S, Steinbach T and Rensberg J 2012 *Phys. Rev.* B **85** 245204
[24] Eckner S, Kämmer H, Steinbach T, Gnauck M, Johannes A, Stephan C, Schorr S and Schnohr C S 2013 *Appl. Phys. Lett.* **103** 081905
[25] Vidal J, Botti S, Olsson P, Guillemoles J-F and Reining L 2010 *Phys. Rev. Lett.* **104** 056401
[26] Wei S-H, Zunger A, Choi I-H and Yu P Y 1998 *Phys. Rev.* B **58** R1710
[27] Botti S, Kammerlander D and Marques M A L 2011 *Appl. Phys. Lett.* **98** 241915
[28] Schnohr C S 2015 *Appl. Phys. Rev.* **2** 031304
[29] Haubold E, Schöppe P, Eckner S, Lehmann S, Colantoni I, d'Acapito F, di Benedetto F, Schorr S and Schnohr C S 2019 *J. Alloys Compd.* **774** 803
[30] Zalewski W, Bacewicz R, Antonowicz J, Pietnoczka A, Evstigneeva T and Schorr S 2010 *J. Alloys Compd.* **492** 35
[31] Welter E, Chernikov R, Herrmann M and Nemausat R 2019 *Conf. Proc.* **2054** 040002
[32] Ravel B and Newville M 2005 *J. Synchrotron Radiat.* **12** 537
[33] Rehr J J, Kas J J, Vila F D, Prange M P and Jorissen K 2010 *Phys. Chem. Chem. Phys.* **12** 5503
[34] Newville M 2013 *J. Phys. Conf. Ser.* **430** 012007
[35] Heyd J, Scuseria G E and Ernzerhof M 2003 *J. Chem. Phys.* **118** 8207
[36] Heyd J, Scuseria G E and Ernzerhof M 2006 *J. Chem. Phys.* **124** 219906
[37] Kresse G and Furthmüller J 1996 *Comput. Mater. Sci.* **6** 15
[38] Kresse G and Furthmüller J 1996 *Phys. Rev.* B **54** 11169
[39] Blöchl P E 1994 *Phys. Rev.* B **50** 17953
[40] Kresse G and Joubert D 1999 *Phys. Rev.* B **59** 1758
[41] Gao F, Yamazoe S, Maeda T, Nakanishi K and Wada T 2012 *Japan. J. Appl. Phys.* **51** 10NC29
[42] Rios L E V, Neldner K, Gurieva G and Schorr S 2016 *J. Alloys Compd.* **657** 408
[43] Balzarotti A, Motta N, Kisiel A, Zimnal-Starnawska M, Czyżyk M T and Podgórny M 1985 *Phys. Rev.* B **31** 7526
[44] León M, Levcenko S, Serna R, Nateprov A, Gurieva G, Merino J, Schorr S and Arushanov E 2013 *Mater. Chem. Phys.* **141** 58
[45] Chen G, Wang W, Chen S, Whang Z, Huang Z, Zhang B and Kong X 2017 *J. Alloys Compd.* **718** 236
[46] Jaffe J E and Zunger A 1984 *Phys. Rev.* B **29** 1882
[47] Schnohr C S 2012 *J. Phys.: Condens. Matter* **24** 325802
[48] Grossberg M, Timmo K, Raadik T, Kärber E, Mikli V and Krustok J 2015 *Thin Solid Films* **582** 176
[49] Zamulko S, Chen R and Persson C 2017 *Phys. Status Solidi* B **254** 1700084
[50] Morihama M, Gao F, Maeda T and Wada T 2014 *Japan. J. Appl. Phys.* **53** 04ER09
[51] Khadka D B and Kim J 2015 *J. Phys. Chem.* C **119** 1706
[52] Bernard J E and Zunger A 1987 *Phys. Rev.* B **36** 3199
[53] Rey G, Redinger A, Sendler J, Weiss T P, Thevenin M, Guennou M, Adib B E and Siebentritt S 2014 *Appl. Phys. Lett.* **105** 112106
[54] Quennet M, Ritscher A, Lerch M and Paulus B 2017 *J. Solid State Chem.* **250** 140